THE JOURNAL OF BIOLOGICAL CHEMISTRY VOL. 287, NO. 18, pp. 14994–15000, April 27, 2012

Dissociation of ATP-binding Cassette Nucleotide-binding Domain Dimers into Monomers during the Hydrolysis Cycle*[S]

Received for publication, January 5, 2012, and in revised form, February 16, 2012 Published, JBC Papers in Press, March 8, 2012, DOI 10.1074/jbc.M112.340281

Maria E. Zoghbi, Srinivasan Krishnan, and Guillermo A. Altenberg[1]

From the Department of Cell Physiology and Molecular Biophysics, and Center for Membrane Protein Research, Texas Tech Health Sciences Center, Lubbock, Texas 79430-6551

Background: In ATP-binding cassette proteins, ATP binding induces formation of nucleotide-binding domain (NBD) dimers, but the mechanism of nucleotide hydrolysis is unknown.
Results: ATP hydrolysis leads to complete separation of NBD dimers, as opposed to dimer opening.
Conclusion: NBD dimers dissociate during the hydrolysis cycle.
Significance: Elucidation of the molecular mechanism of hydrolysis will help us understand the function of ATP-binding cassette proteins.

ATP-binding cassette (ABC) proteins have two nucleotide-binding domains (NBDs) that work as dimers to bind and hydrolyze ATP, but the molecular mechanism of nucleotide hydrolysis is controversial. In particular, it is still unresolved whether hydrolysis leads to dissociation of the ATP-induced dimers or opening of the dimers, with the NBDs remaining in contact during the hydrolysis cycle. We studied a prototypical ABC NBD, the *Methanococcus jannaschii* MJ0796, using spectroscopic techniques. We show that fluorescence from a tryptophan positioned at the dimer interface and luminescence resonance energy transfer between probes reacted with single-cysteine mutants can be used to follow NBD association/dissociation in real time. The intermonomer distances calculated from luminescence resonance energy transfer data indicate that the NBDs separate completely following ATP hydrolysis, instead of opening. The results support ABC protein NBD association/dissociation, as opposed to constant-contact models.

ABC[2] proteins constitute one of the largest protein superfamilies, expanding from bacteria to humans, with most members corresponding to membrane proteins that mediate transmembrane substrate transport (1). Elucidation of the mechanism of ABC proteins is essential to understand processes such as multidrug resistance of cancer cells mediated by P-glycoprotein (MDR1, ABCB1), as well as genetic diseases such as cystic fibrosis, caused by mutations of CFTR, the cystic fibrosis transmembrane conductance regulator (ABCC7) (1, 2).

The core structure of ABC proteins comprises two transmembrane domains and two NBDs (1). The NBDs, the engines of ABC proteins, are responsible for nucleotide binding and hydrolysis, and their structure is conserved among ABC proteins with dissimilar functions (1). It has been established that ATP binding induces formation of dimers with two ATPs sandwiched at the dimer interface (3, 4). Each nucleotide-binding site is formed by residues from both NBDs (see Fig. 1*A*). Despite the detailed structural knowledge of the NBDs, the mechanism of nucleotide hydrolysis is controversial. As a result of experimental discrepancies and lack of direct information, a number of models have been proposed (3–14). These models can be broadly divided into the following. 1) In monomer/dimer models, where ATP hydrolysis is followed by dissociation of the dimers, and the energy that drives the conformational changes that lead to substrate transport (power stroke) is provided by the dimer association-dissociation. 2) Constant-contact models, where the NBDs remain in contact during the hydrolysis cycle, and the power stroke results from smaller conformational changes at the NBD-dimer interface.

Here, we studied the association and dissociation of a well studied NBD, the *Methanococcus jannaschii* MJ0796 (4, 9, 15, 16), with two independent spectroscopic techniques to follow the oligomeric state of the NBDs in real time. We used tryptophan fluorescence quenching and luminescence resonance energy transfer (LRET) to follow the monomer/dimer state in real time and determined intermonomer distances during the hydrolysis cycle using LRET. Our results support hydrolysis models that include separation of NBD dimers into monomers during the ATP hydrolysis cycle.

EXPERIMENTAL PROCEDURES

Protein Expression and Purification—Three mutants of the *M. jannaschii* MJ0796 were expressed in *Escherichia coli* and purified: 1) Cys-less-MJ0796-G174W (MJ-CL, in which[3] Cys-53 and Cys-128 were replaced with Gly and Ile, respectively, which are the residues in the equivalent positions of the *M. jannaschii* MJ1267 NBD, and Gly-174 was replaced with

* This work was supported, in whole or in part, by National Institutes of Health Grants R01GM79629 and 3R01GM079629-03S1 (to G. A. A.). This work was also supported by Cancer Prevention and Research Institute of Texas Grant RP101073.

[S] This article contains supplemental Methods, Figs. 1–5, and supplemental Table 1.

[1] To whom correspondence should be addressed. Tel.: 806-743-2531; E-mail: g.altenberg@ttuhsc.edu.

[2] The abbreviations used are: ABC, ATP-binding cassette; LRET, luminescence resonance energy transfer; NBD, nucleotide-binding domain; DTPA, diethylenetriaminepentaacetate.

[3] The following mutant designations were used throughout this study: MJ-CL, Cys-less, single-Trp MJ0796 mutant (MJ0796-C53G-C128I-G174W); MJ-C14, single-Cys mutant (G14C) on the MJ-CL background; and MJI-C14, catalytically deficient mutant (E171Q) on the MJ-C14 background.

Trp); 2) single-Cys MJ0796-G174W-G14C (MJ-C14); and 3) single-Cys MJ0796-G174W-E171Q-G14C (MJI-C14). MJ-CL DNA was synthesized (GenScript, Piscataway, NJ), and the other mutants were obtained by site-directed mutagenesis. DNAs were cloned into pET19b (EMD Biosciences, Rockland, MA) for expression in *E. coli* BL21-CodonPlus (DE3)-RILP (Agilent Technologies, Santa Clara, CA). Induction was with 1 mM isopropyl-β-D-thiogalactopyranoside for 2 h at 37 °C. Proteins were purified as described (16), with all procedures carried out at 4 °C. Basically, cells were disrupted in 50 mM NaCl, 1 mM EDTA, 4 mM DTT, and 50 mM Tris/HCl, pH 7.6 (lysis buffer), with 1 mM PMSF. The lysate was centrifuged for 15 min at 30,000 × *g*, and the supernatant was diluted 2-fold with NaCl-free buffer (1 mM EDTA, 1 mM DTT, 50 mM Tris HCl, pH 7.6), filtered, and loaded into a Mono Q anion-exchange column (HiPrepQ FF16, GE Healthcare). Elution was accomplished with a linear 0–1 M [NaCl] gradient. The highly purified protein can be used for biochemical and biophysical studies, but a homogeneous monodisperse pure sample can be obtained after additional purification by gel filtration using a Superdex HR200 10/300 GL column (GE Healthcare, see supplemental Methods). Purified proteins were stored at −80 °C.

Tryptophan Fluorescence Measurements—Changes in Trp fluorescence (1–2 μM protein in 200 mM NaCl, 1 mM EDTA, 10% glycerol, and 50 mM Tris/HCl, pH 7.6) were determined at 20 °C, with excitation at 295 nm. Depending on the experiment, we recorded emission spectra between 310 and 400 nm or emission at 345 nm (Hitachi F-7000 spectrofluorometer, Tokyo, Japan).

LRET Studies—Single-Cys mutants MJ-C14 and MJI-C14 in 1 mM EDTA, 50 mM Tris, pH 7.6, were labeled with the thiol-reactive Tb^{3+} chelate DTPA-cs124-EMPH (17), fluorescein maleimide (Invitrogen), or Cy3 maleimide (GE Healthcare), at a 2-to-1 molar excess. DTPA-cs124-EMPH contains carbostyril 124 (7-amino-4-methyl-2(1*H*)-quinolinone) as an "antenna" that absorbs at 335 nm, the chelator diethylenetriaminepentaacetate (DTPA) that binds Tb^{3+} tightly and shields it from the quenching effects of water, and the thiol-selective maleimide group for protein labeling. MJ-CL was used as control to determine nonspecific labeling. NBDs were labeled with donor or with acceptor for 2 h at room temperature, and unreacted probes were removed by gel filtration (Zeba columns, Thermo Fisher Scientific). For some LRET studies, the labeled monomers were further purified by gel filtration on a Superdex 200HR column. For the basic protocol, we split the single-Cys monomers and labeled one-half with donor (Tb^{3+}-chelate maleimide) and the other half with acceptor (fluorescein maleimide or Cy3 maleimide). Donor-labeled and acceptor-labeled NBDs were mixed at a one-to-one molar ratio prior to LRET experiments, and the proximity between the donor- and acceptor-labeled monomers was determined under different conditions. Emission was measured on either a Photon Technology International spectrometer (QM3SS, Photon Technology International, Inc., London, Ontario, Canada) or an Optical Building Blocks phosphorescence lifetime photometer (EasyLife L, Optical Building Blocks Corp., Birmingham, NJ). The emission was recorded with a 200-μs delay from the beginning of the ~1-μs excitation pulse from a xenon flash lamp (gated mode). During those 200 μs, the short lifetime processes such as acceptor emission resulting from direct excitation, scattering of the excitation pulse, and autofluorescence decay significantly. Therefore, in gated mode, the remaining light arises from long lifetime processes such as emission from the donor or sensitized emission from the acceptor. Excitation was set to 335 nm with a monochromator in the Photon Technology International system or by the use of a narrow band 335-nm filter (Semrock FF01-335/7, Rochester, NY) in the Optical Building Blocks system. Emission spectra were recorded with the Photon Technology International system. For intensity measurements, we used band-pass filters (Omega Optical, Brattleboro, VT) appropriate to collect light from Tb^{3+} (490/10 nm), fluorescein (520/10 nm) or Cy3 (570/10). Generally, donor and acceptor emission decays were collected as averages from 1,800 pulses at 100 Hz. As expected, donor emission and sensitized acceptor emission were not polarized (supplemental Fig. 5).

Distances between the donor and acceptor probes were calculated according to

$$E = 1 - \tau_{DA}/\tau_D \quad \text{(Eq. 1)}$$

$$R = R_0\,(E^{-1} - 1)^{1/6} \quad \text{(Eq. 2)}$$

where E is the efficiency of energy transfer, R_0 is the Förster distance (the distance at which $E = 0.5$), and τ_D and τ_{DA} are the lifetimes of the donor in the absence and presence of the acceptor, respectively. In LRET, the lifetime of the donor molecules that participate in energy transfer, τ_{DA}, is equal to the sensitized emission lifetime, *i.e.* the long lifetime of the acceptor that arises exclusively from energy transfer (18). The donor-only decay (τ_D) was well fitted by a two-exponential decay function, where the fast component ($\tau = 664 \pm 64$ μs, $n = 10$) contributed only 5 ± 1% to the signal. Therefore, only the slower lifetime ($\tau = 2{,}088 \pm 7$ μs) was used for the distance calculations, but using a weighted average of the lifetimes yielded calculated distances that differed from the values reported under "Results" by <1 Å. For the determination of the donor-acceptor lifetimes (τ_{DA}), we first eliminated the contribution of the ATP-insensitive components by subtracting the decays in ATP and Mg-ATP from the decay in the absence of ATP (decays from the same sample in different conditions: no ATP, after the addition of ATP, and after the subsequent addition of Mg^{2+}). This maneuver allowed us to fit the sensitized emission decays to a single exponential function (after 800 μs for the Tb^{3+}/fluorescein pair or after 500 μs for the Tb^{3+}/Cy3 pair), which simplified the analysis and interpretation of the data because the lifetime can be ascribed to a single donor-acceptor distance. Additional details on the analysis of LRET data are presented under the supplemental Methods.

Data Presentation and Statistics—Data are shown as means ± S.E. Statistical comparisons were performed by the Student's *t* test for paired or unpaired data, as appropriate. $p < 0.05$ in a two-tailed analysis was considered significant. The number of experiments, *n*, corresponds to independent measurements from at least three different protein preparations. The goodness of fit for the analysis of LRET decays was deter-

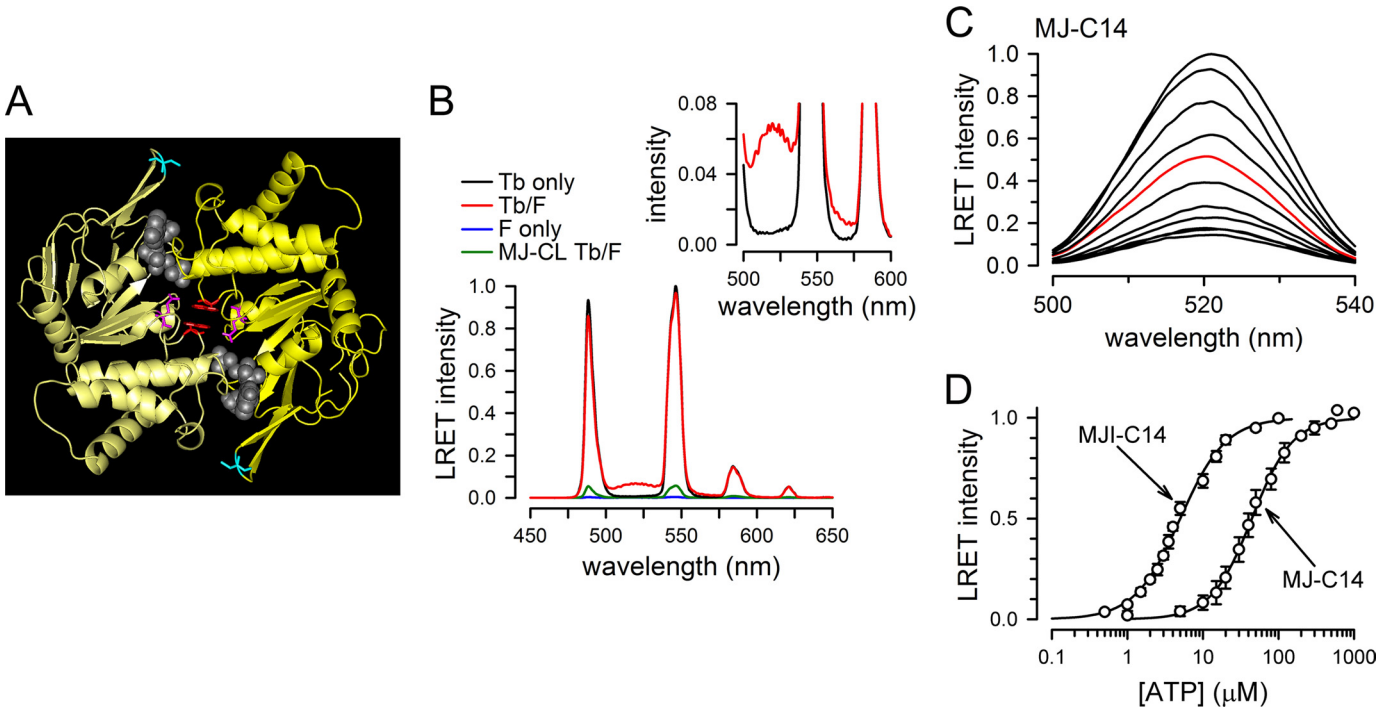

FIGURE 1. **Structure and function of NBDs.** *A*, structure of nucleotide-bound MJI-C14. Each monomer is represented in a different *yellow tone*. ADP and P_i are shown in space-filling representation (*gray*), and Cys-14, Gln-171, and Trp-174 are shown in sticks representation (*cyan*, *magenta*, and *red*, respectively). This structure is based on the MJ0796-E171Q/G174W coordinates (Protein Data Bank (PDB) 3TIF). *B*, emission spectra from ATP-bound MJ-C14 dimers labeled with Tb^{3+} only (*Tb only*, *black*), fluorescein only (*F only*, *blue*), or Tb^{3+} and fluorescein (*Tb/F*, *red*). The emission spectrum of MJ-CL subjected to the Tb^{3+}/fluorescein labeling procedure is also shown *(MJ-CL Tb/F*, *green trace*). The *inset* is a zoomed view showing the donor only (*black*) and donor-acceptor traces (*red*). Protein concentration was 2 μM, and 2 mM ATP was added 10 min before collecting the spectra. Intensities were normalized to the 546-nm MJ-C14 Tb/F Tb^{3+} peak, except for the Tb^{3+} only trace, which was scaled to the Tb^{3+} 585-nm peak of MJ-C14 Tb/F. *C*, typical MJ-C14 LRET intensity changes in response to increasing ATP concentration. The sensitized fluorescein emission was measured at ATP concentrations ranging from zero (*bottom trace*) to 500 μM (*top trace*). Intermediate ATP concentrations were 5, 10, 15, 20, 30, 40 (*red*), 50, 100, 200, and 500 μM. Traces correspond to data normalized to the peak emission in 500 μM ATP. The spectra were acquired at 5-min intervals between sequential ATP additions. The solutions were nominally divalent cation-free and contained 1 mM EDTA, to prevent ATP hydrolysis. *D*, summary of the dependence of the LRET signal on ATP concentration. The sensitized emission data were obtained from experiments similar to those in *panel C* and are shown as means ± S.E. (n = 5 for each protein). S.E. values smaller than the symbol size are not shown.

mined from the random residual distribution, which showed no structure and χ-square values near unity.

RESULTS

Monitoring ATP-induced Dimerization by LRET—We engineered single-Cys mutants (Gly-14 to Cys), starting with a Cys-less background (MJ-CL). One of the mutants (MJ-C14) is catalytically active, whereas the other mutant (MJI-C14) is inactive (E171Q substitution). The Glu-171 to Gln mutation essentially abolishes ATP hydrolysis and stabilizes ATP-induced dimerization (4, 15, 16). The single-Cys mutants also have an introduced Trp at position 174, which has been shown to be a good dimerization probe (16), to allow for parallel assessment of dimerization by Trp quenching. Fig. 1*A* shows the residues Glu-171 and Trp-174 in the nucleotide-bound MJI dimer crystal structure (16) and illustrates the position of Cys-14. In most experiments, we used the Tb^{3+}/fluorescein LRET donor-acceptor pair because its R_0 of 46.2 Å is close to the estimated Cys-14-Cys-14 distance in the dimer structure (50 Å). We also performed experiments using the Tb^{3+}/Cy3 pair (R_0 = 61.2 Å). Single-Cys mutants were well labeled with the LRET probes (as shown in SDS-PAGE gels on a UV transilluminator), and analysis of the NBD oligomeric state by size-exclusion chromatography indicated that the single-Cys mutants are able to dimerize in the presence of ATP even after labeling with the LRET probes (supplemental Fig. 1). The behavior of MJ-C14 and MJI-C14 in size-exclusion chromatography is indistinguishable from that of the corresponding MJ and MJI proteins (16).

The emission spectra from labeled NBDs in 2 mM ATP are shown in Fig. 1*B*. The Tb^{3+}-labeled NBD spectrum (*black trace*, *Tb only*) shows sharp peaks with interposed dark regions, typical of the emission of this lanthanide. The fluorescein-labeled NBDs (*blue trace*, *F only*) showed basically no emission, demonstrating that gating of the emission recording effectively removes nanosecond-lifetime processes such as direct excitation of the acceptor. When Tb^{3+}-labeled and fluorescein-labeled NBDs were mixed, the emission spectrum (*red trace*, *Tb/F*) showed the typical Tb^{3+} peaks plus an emission that peaked at 520 nm corresponding to the sensitized emission of fluorescein (see *inset* for a zoomed view), *i.e.* fluorescein emission resulting from its excitation by energy transfer from Tb^{3+}. The emission spectrum for the similarly Tb^{3+}/fluorescein-labeled MJ-CL (*green trace*, *MJ-CL Tb/F*) showed small peaks corresponding to Tb^{3+} emission from basal unspecific labeling and/or unbound Tb^{3+} remaining after gel filtration, but sensitized fluorescein emission was undetectable. Therefore, the fluorescein signal measured in MJ-C14 and MJI-C14 arises from energy transfer between the probes bound to Cys-14. ATP

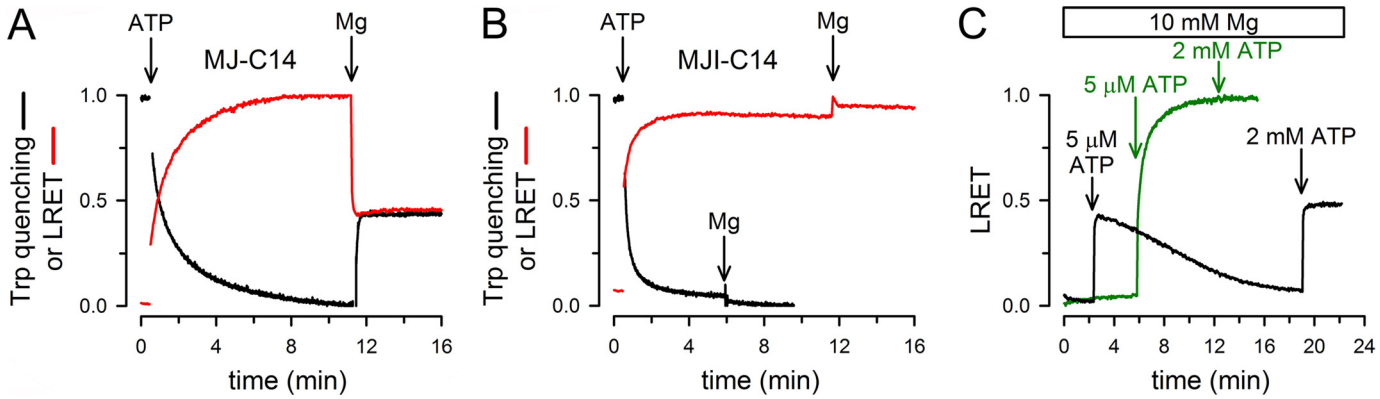

FIGURE 2. **Time course of NBD association/dissociation monitored by LRET and Trp quenching.** *A*, changes in MJ-C14 Trp fluorescence (*black*) and fluorescein sensitized emission (*red*) in response to ATP and Mg-ATP. MJ-C14 used to detect Trp fluorescence was not labeled with LRET probes. ATP (2 mM) was added at the *first arrow*, and $MgCl_2$ (10 mM) was added at the *second arrow*. Traces show signals normalized to the total change. *B*, changes in MJI-C14 Trp fluorescence (*black*) and fluorescein sensitized emission (*red*) in response to ATP and Mg-ATP. See *panel A* for details. *C*, response of MJ-C14 (*black*) and MJI-C14 (*green*) LRET signal to low Mg-ATP concentration. Mg^{2+} at a concentration of 10 mM was present from the beginning. For all panels, the protein concentration was 2 μM, and the traces are representative of data from >5 similar experiments.

had no significant effect on the emission of MJ-CL, Tb^{3+}-only, or acceptor-only NBDs. Equivalent results were obtained for the Tb^{3+}/Cy3 LRET pair, where a clear Cy3 sensitized emission peak at 565 nm can be observed (supplemental Fig. 2).

The dependence of the fluorescein sensitized emission on ATP concentration is shown in Fig. 1*C*. Mixed Tb^{3+}- and fluorescein-labeled MJ-C14 in the absence of ATP showed a small emission that gradually increased as the NBDs were exposed to increasing ATP levels. This ATP-dependent increase in sensitized emission originates from the association between Tb^{3+}-labeled and fluorescein-labeled monomers that, after binding ATP, become close enough (dimerize) to allow energy transfer between the donor and acceptor. If random association between monomers occurs after the addition of ATP, the sensitized emission originates from a representative sample of the dimers; those formed by a Tb^{3+} monomer and a fluorescein monomer. Because the recorded acceptor emission with long lifetime can only arise from energy transfer, the stoichiometry of labeling affects the intensity of the signal, but not the distance calculations or the K_d determinations, which depend on relative changes and probe lifetimes, respectively (18, 19). In the absence of ATP, basically all NBDs are in monomeric form (supplemental Fig. 1); thus, the small fluorescein signal observed before the addition of ATP is mostly due to scattering of the excitation pulse (artifact that depends on the instrument response time) and to the presence of a small fraction of aggregates (see supplemental Methods). From the ATP-dependent increment in the sensitized fluorescein emission, we calculated the apparent affinity constants for ATP of MJ-C14 (K_d = 47 ± 3 μM, n = 5) and MJI-C14 (K_d = 5.0 ± 0.2 μM, n = 5), with Hill coefficients of 1.6 ± 0.1 and 1.4 ± 0.1, respectively (Fig. 1*D*). The ~10-fold increased affinity for ATP of MJI-C14 has been previously reported for other E171Q mutants (15, 16). The apparent affinities for ATP and Hill coefficients determined by Trp fluorescence quenching in MJ-C14 and MJI-C14 were close to the values determined by LRET (supplemental Fig. 3) and to those previously found for the corresponding active and inactive proteins with the native Cys residues (16). This indicates that removal of the two native Cys residues and introduction of a single-Cys mutation at position 14 does not result in significant alterations in ATP binding and dimerization. In addition, the similarity between the ATP-induced responses of LRET and Trp-174 fluorescence supports the notion that these two independent techniques can be used to monitor NBD dimerization.

Dynamic Dimerization and Dissociation of NBDs—The time courses of the changes in fluorescein sensitized emission and Trp-174 fluorescence in response to a saturating concentration of ATP are shown in Fig. 2, *A* (MJ-C14) and *B* (MJI-C14). The changes in sensitized emission (*red trace*) and Trp fluorescence (*black trace*) followed the same time course, but had opposite direction; dimerization causes Trp fluorescence quenching by Trp-174-Trp-174 π stacking (16), whereas it increases fluorescein emission by bringing the donor- and acceptor-labeled monomers closer. Dimerization of MJ-C14 and MJI-C14 proceeded slowly, requiring several minutes for completion. The dimerization of MJ-C14 induced by Na-ATP was ~3-fold slower than the corresponding MJI-C14 dimerization (Fig. 2*B* *versus* Fig. 2*A*, see supplemental Table 1). We have previously found that the slow rate of NBD dimerization induced by Na-ATP is not due to mixing artifacts or limiting NBD concentration (16). Also, in agreement with previous results (16), we found a dramatic increase in the dimerization rate of MJ-C14 by Mg-ATP *versus* Na-ATP, an effect absent in MJI-C14 (see supplemental Table 1). The similarity of these observations with the responses of active and inactive MJ0796 (16) suggests that the single-Cys mutants behavior is essentially identical to that of the NBDs containing the native Cys.

The reason for the faster Mg-ATP- *versus* Na-ATP-induced dimerization of catalytically active MJ0796 has not been established, but Mg^{2+} coordination at the active site and electrostatics at the dimer interface could play a role (4). In many NTPases, including ABC NBDs, the conserved acidic residue at the end of the Walker B motif (Glu-171 in MJ0796) makes a water-mediated contact with Mg^{2+}, required for high affinity nucleotide binding (20, 21). The nucleotide-bound dimer interface has a relatively intense concentration of negative charge, and Mg^{2+} coordination could facilitate ATP binding and NBD associa-

tion. If electrostatics at the dimer interface are important for dimerization, it is possible that the absence of the Glu negative charge in the E171Q mutant facilitates Na-ATP-induced dimerization and accounts for the faster MJI-C14 dimerization by Na-ATP.

Fig. 2*A* also shows that after the addition of Mg^{2+} to MJ-C14, there was a fast decrease of fluorescein sensitized emission and increase of Trp fluorescence (see also supplemental Table 1). The LRET signal and Trp emission reached a stable value approximately halfway between the 100% monomer (*No ATP*) and the 100% dimer signals (in saturating ATP). When compared with ATP alone, reversals of LRET signal and Trp quenching were 60 ± 3% (n = 11) and 51 ± 1% (n = 11), respectively. These intermediate values in Mg-ATP are the result of the increased distance between NBDs labeled with LRET probes (~50% of the dimers dissociate, see section below) and break of the Trp-174-Trp-174 π stacking, respectively, and represent a new steady state where only ~50% of the NBDs are present as dimers. The effect of Mg^{2+} depended on ATP hydrolysis because it was absent in MJI-C14 (Fig. 2*B*). In addition, the rate constant of the Mg^{2+}-induced increase in MJ-C14 Trp emission was ~0.2 s^{-1} ($1/\tau$ in supplemental Table 1), comparable with the measured rate of ATP hydrolysis (0.2 s^{-1}). In summary, the addition of ATP alone induces dimerization of 100% of the NBDs, and the subsequent addition of Mg^{2+} to MJ-C14 promotes hydrolysis, inducing NBD dissociation into monomers. Because the hydrolytic activity is insufficient to decrease the [ATP] below saturation level (the K_d for Mg-ATP-induced dimerization is ~5 μM, see Ref. 16), NBDs reassociate rapidly, leading to a dynamic monomer/dimer equilibrium with continuous ATP hydrolysis (16). The rapid reassociation is a consequence of the increased association speed elicited by Mg-ATP *versus* Na-ATP (supplemental Table 1).

The relationship between changes in LRET signal and ATP hydrolysis is also apparent in the experiments shown in Fig. 2*C*. The addition of a low concentration of ATP (5 μM) to 2 μM MJ-C14 in the presence of Mg^{2+} induced a fast and transient increase in sensitized emission (*black trace*). Because the K_d for Mg-ATP is expected to be at least 10-fold lower than for Na-ATP (16), this low Mg-ATP concentration was able to induce significant NBD dimerization. However, after reaching a maximum, the signal slowly returned toward the pre-ATP value. The subsequent addition of 2 mM ATP produced a stable increase in LRET, similar to the steady-state intensity in 2 mM Mg-ATP shown in Fig. 2*A*. In MJI-C14 (*green trace*), a low concentration of Mg-ATP produced a stable LRET signal increase (corresponding to ~100% dimers) that did not change significantly after the subsequent addition of 2 mM ATP. These results suggest that the LRET signal follows the time course of the changes in ATP concentration. It seems likely that for MJ-C14, but not MJI-C14, the initial 5 μM ATP concentration decreases as a consequence of ATP hydrolysis by the NBDs until there is not enough ATP to elicit rapid redimerization of the monomers. At 2 mM ATP, the decrease in ATP concentration during the experiment is insufficient to reduce ATP below saturation, resulting in a stable maximal change. Similar response of MJ-C14 and MJI-C14 to low Mg-ATP concentrations was obtained when their dimerization was monitored by Trp-174 quenching and was also observed for the native Cys-containing NBDs (16), suggesting that labeling with the LRET probes does not have a major effect on the dynamics of the association/dissociation of the protein. In summary, the results suggest that LRET and Trp-174 quenching allow for monitoring the association/dissociation cycle of a catalytically active NBD in real time.

Determination of Intermonomer Distances—In addition to its usefulness for monitoring NBD dimerization, LRET can be used to determine the distances that separate the donor and acceptor bound to the protein. Distances are calculated from the lifetimes of sensitized emission decays, as described under "Experimental Procedures." Fig. 3*A* shows the millisecond (τ = 2,088 ± 7 μs) emission decay of Tb^{3+}-labeled MJ-C14 (*black trace*, recorded at 490 nm). When Tb^{3+}- and fluorescein-labeled MJ-C14 were mixed in the presence of 2 mM ATP, a fluorescein sensitized emission decay (*red trace*, recorded at 520 nm) faster than the Tb^{3+}-only emission decay was observed, as expected from energy transfer. Tb^{3+}- and fluorescein-labeled MJ-C14 mixed in the absence of ATP showed much less fluorescein sensitized emission intensity (*blue trace*). For analysis, this ATP-independent component was subtracted from the ATP-dependent sensitized emission. Sensitized emission from MJ-CL subjected to the Tb^{3+} and fluorescein labeling procedure was negligible, confirming that the sensitized emission measured in MJ-C14 arises from Cys-14 labeled with the optical probes. An ATP-dependent Cy3 sensitized emission was also observed (Fig. 3*B*). The fluorescein and Cy3 sensitized emission lifetimes and the distances calculated for the Tb^{3+}/fluorescein and Tb^{3+}/Cy3 LRET pairs are shown in Table 1. The shorter lifetime of the Cy3 sensitized emission when compared with the one from fluorescein (364 ± 30 *versus* 1,266 ± 14 μs) results from the differences in R_0 (46 Å *versus* 61 Å for Tb^{3+}/fluorescein and Tb^{3+}/Cy3, respectively), but the calculated donor-acceptor distance was very similar. In the dimers formed in 2 mM ATP, the donor-acceptor distance was 49.7 ± 0.2 Å using Tb^{3+}/fluorescein pair data and 47.1 ± 0.8 Å using data from the Tb^{3+}/Cy3 pair. The donor-acceptor distances in 2 mM ATP are in good agreement with the 50 Å Cys-14-Cys-14 distance estimated from the dimer structure. The slightly shorter distance calculated from the Tb^{3+}/Cy3 *versus* Tb^{3+}/fluorescein data is likely due to the difference in size of Cy3 *versus* fluorescein.

We also calculated donor-acceptor distances from the sensitized emission decays recorded in the presence of 2 mM Mg-ATP. Table 1 shows that the Tb^{3+}/fluorescein distance after the addition of Mg^{2+} was 49.0 ± 0.4, identical to the distance calculated in the absence of Mg^{2+}. This result clearly indicates that although the intensity of the MJ-C14 sensitized emission decreases ~60% after the addition of Mg^{2+} (Fig. 2*A*), the intermonomer distance remains constant. The total ATP-dependent fluorescein sensitized emission from ATP-induced dimers decreased 59 ± 11% after the addition of Mg^{2+} (n = 5), consistent with the Trp and LRET intensity changes presented earlier (60 ± 3%). This ~60% decrease in LRET intensity can be accounted for by an increase in the donor-acceptor distance of ~8 Å, which would require an increase in the fluorescein sensitized emission lifetime from 1,266 to ~1,660 μs. If present, a change of this magnitude should be easily detectable. However,

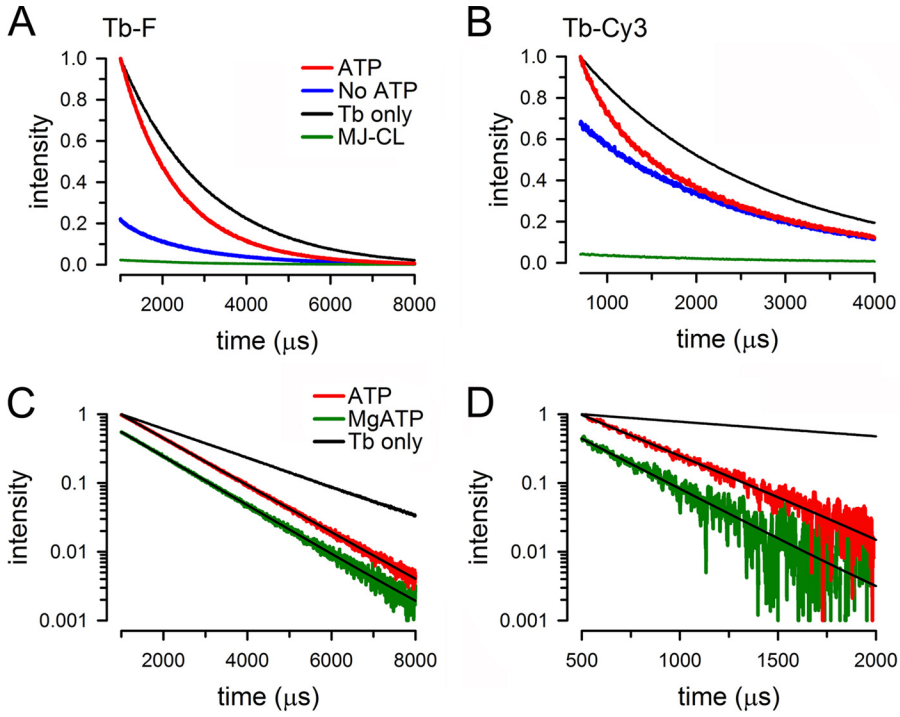

FIGURE 3. **Emission decays of donor- and donor-acceptor-labeled NBDs.** *A*, effect of ATP on sensitized fluorescein emission decay from MJ-C14. *Black trace* (*Tb only*), emission of MJ-C14 labeled with Tb^{3+} only, measured at 490 nm. *Blue* (*No ATP*) and *red traces* (*ATP*), sensitized fluorescein emission of MJ-C14 labeled with Tb^{3+} and fluorescein, measured at 520 nm in the absence or presence of 2 mM ATP, respectively. *Green trace* (*MJ-CL*), sensitized fluorescein emission (measured at 520 nm) of Cys-less protein (MJ-CL) subjected to the Tb^{3+} and fluorescein labeling procedure. When present, ATP concentration was 2 mM. Tb^{3+} only and ATP intensities were normalized to their corresponding values at 1,000 μs, and the *No ATP* and *MJ-CL* intensities were normalized to the ATP intensity at 1,000 μs. The traces are representative of 5 similar experiments. *B*, effect of ATP on sensitized Cy3 emission decay from MJ-C14. Details are as in *panel A*, but Cy3 was used as acceptor instead of fluorescein, with the sensitized emission measured at 570 nm. *C*, effect of Mg-ATP on the sensitized fluorescein emission decay of Tb^{3+}/fluorescein-labeled MJ-C14. Semilog plot of the sensitized fluorescein decay measured in 2 mM ATP (*red*) and after the addition of $MgCl_2$ (*green*). The decay in the absence ATP (recorded in the same sample at the beginning of the experiment) was subtracted from the ATP and Mg-ATP decays, resulting in traces that can be fit to a single exponential function (*black lines* over the ATP and Mg-ATP traces). The decay from MJ-C14 labeled with Tb^{3+} alone (*black*) is also shown. ATP and Tb^{3+} only were normalized to their intensities at 1,000 μs, whereas the Mg-ATP data were normalized to the ATP intensity at 1,000 μs. *D*, effect of Mg-ATP on the sensitized Cy3 emission decay of Tb^{3+}/Cy3-labeled MJ-C14. Details are as in *panel C*, but Cy3 was used as acceptor instead of fluorescein.

TABLE 1

Summary of LRET lifetimes and calculated distances

ATP: 2 mM Na-ATP; Mg-ATP: 2 mM Mg-ATP; Tb^{3+}/F and Tb^{3+}/Cy3: Tb^{3+}/fluorescein and Tb^{3+}/Cy3; τ: lifetime; *R*: donor-acceptor distance; *n*: number of independent measurements. Data are presented as means ± S.E., except for the Tb^{3+}/Cy3 Mg-ATP data, where the average of two experiments is shown.

	LRET pairs					
	Tb^{3+}/F			Tb^{3+}/Cy3		
	τ	R	*n*	τ	R	*n*
	μs	Å		μs	Å	
ATP	1266 ± 14	49.6 ± 0.2	5	364 ± 30	47.1 ± 0.8	6
Mg-ATP	1224 ± 23	49.0 ± 0.4	4	231	42.9	2

the sensitized emission decay lifetimes observed in 2 mM ATP and 2 mM Mg-ATP were indistinguishable, as clearly visualized by the essentially parallel decays in the semilog plot of Fig. 3*C*. Even in the extreme case of the experiment shown in supplemental Fig. 4, where the addition of Mg^{2+} decreased the LRET intensity more than 80%, no change in the decay lifetime was observed. To corroborate the absence of changes, we performed two experiments using Cy3 as acceptor. The increase in distance of ~8 Å necessary to explain the 60% decrease in the fluorescein sensitized emission intensity requires an increase in the Cy3 sensitized emission lifetime from 364 to ~725 μs. Again, no such change was observed (Fig. 3*D*). This lack of significant changes in sensitized emission decay lifetimes indicates that the decrease in the intensity of the LRET signal under conditions that promote ATP hydrolysis is the result of a decrease in dimer concentration, without changes in the intermonomer distance.

DISCUSSION

We recently showed that ATP induces Trp fluorescence quenching in MJ0796 variants with the G174T substitution, as a result of NBD dimerization (16). Protein Trp spectroscopy is very useful because Trp is a small genetically encoded probe that does not require labeling, and therefore, the stoichiometry is well defined. However, the Trp quantum yield is low when compared with "bright" fluorophores such as fluorescein, and its use in membrane protein studies (*e.g.* for future application to full-length ABC proteins) is limited by light scattering from protein-detergent complexes or proteoliposomes. To overcome these drawbacks, we tested NBD dimerization by LRET in MJ-C14 and MJI-C14. For LRET, we used the rare element Tb^{3+}, characterized by a long lifetime emission, as donor (18). LRET has been used previously to assess intersubunit and intramolecular distances in various proteins (19, 22–26). LRET has many advantages for our experiments when compared with traditional fluorescence resonance energy transfer (19). These advantages include a very low background, high signal-to-noise ratio, and independence of the labeling stoichiometry, enabling

LRET to measure distances in the 25–100 Å range with little uncertainty due to orientation factors (19). The residue at position 14 (Cys-14) was chosen as the target for labeling because it is a surface residue exposed to the aqueous solvent (available for labeling), it is not part of the active site or dimer interface (Fig. 1*A*), and the expected Cys-14-Cys-14 distance in the dimer (4, 14) is compatible with LRET (19). We primarily used the Tb^{3+}/fluorescein donor-acceptor pair because its Förster distance is 46.2 Å, close to the distance between the Cys-14-Cys-14 side chains in the dimers (~50 Å). Because of the dependence of LRET on the sixth power of the distance between the probes, the experimental conditions ensure detection of a separation of a few Å and minimal signal between monomers in solution.

The results in the present work indicate that NBD dimerization can be monitored by both Trp-174 fluorescence and LRET. In the absence of Mg^{2+}, ATP slowly induces a stable dimerization of the NBDs, which can be observed as 1) quenching of Trp-174 fluorescence due to the π-stacking of the Trps (Fig. 1*A*) (16) and 2) an increase in LRET signal due to the increased proximity of donor- and acceptor-labeled monomers. The addition of Mg^{2+} promotes hydrolysis of ATP by the dimers and reverses 50–60% of the ATP-induced Trp quenching and LRET signal. Such reversion might be explained by 1) a decrease in the proportion of dimeric NBDs (complete NBD separation, as expected from the association/dissociation model) or 2) by opening of the dimers (dimers remain in contact, constant-contact model). In the first case, dimer population would decrease from 100% in 2 mM ATP to ~40–50% in 2 mM Mg-ATP, whereas the sensitized emission lifetime, which depends on the sixth power of the donor-acceptor distance, will remain unchanged. In the second case, opening of the dimers would increase the donor-acceptor distance, reducing the efficiency of energy transfer. Such decreased efficiency would lower the LRET signal intensity and would make the sensitized emission lifetime longer. Our LRET distance calculations strongly favor the first scenario, and therefore, support the ABC NBD hydrolysis models that include association/dissociation, as opposed to constant-contact models.

In summary, the LRET data demonstrate that ATP hydrolysis leads to complete separation of the dimers, as opposed to opening. Future studies using the spectroscopic techniques presented here can determine whether the NBD association/dissociation or constant-contact models explain the hydrolysis cycle of full-length ABC proteins.

Acknowledgments—We thank Drs. Luis Reuss and Ina Urbatsch and Rebecca Sisson-Cooper for discussions and comments on the manuscript.

REFERENCES

1. Bouige, P., Laurent, D., Piloyan, L., and Dassa, E. (2002) Phylogenetic and functional classification of ATP-binding cassette (ABC) systems. *Curr. Protein Pept. Sci.* **3,** 541–559
2. Sharom, F. J. (2008) ABC multidrug transporters: structure, function, and role in chemoresistance. *Pharmacogenomics* **9,** 105–127
3. Hopfner, K. P., Karcher, A., Shin, D. S., Craig, L., Arthur, L. M., Carney, J. P., and Tainer, J. A. (2000) Structural biology of Rad50 ATPase: ATP-driven conformational control in DNA double-strand break repair and the ABC-ATPase superfamily. *Cell* **101,** 789–800
4. Smith, P. C., Karpowich, N., Millen, L., Moody, J. E., Rosen, J., Thomas, P. J., and Hunt, J. F. (2002) ATP binding to the motor domain from an ABC transporter drives formation of a nucleotide sandwich dimer. *Mol. Cell* **10,** 139–149
5. Chen, J., Lu, G., Lin, J., Davidson, A. L., and Quiocho, F. A. (2003) A tweezers-like motion of the ATP-binding cassette dimer in an ABC transport cycle. *Mol. Cell* **12,** 651–661
6. Dawson, R. J., and Locher, K. P. (2006) Structure of a bacterial multidrug ABC transporter. *Nature* **443,** 180–185
7. Higgins, C. F. (2007) Multiple molecular mechanisms for multidrug resistance transporters. *Nature* **446,** 749–757
8. Janas, E., Hofacker, M., Chen, M., Gompf, S., van der Does, C., and Tampé, R. (2003) The ATP hydrolysis cycle of the nucleotide-binding domain of the mitochondrial ATP-binding cassette transporter Mdl1p. *J. Biol. Chem.* **278,** 26862–26869
9. Jones, P. M., and George, A. M. (2009) Opening of the ADP-bound active site in the ABC transporter ATPase dimer: evidence for a constant contact, alternating sites model for the catalytic cycle. *Proteins* **75,** 387–396
10. Sauna, Z. E., Kim, I. W., Nandigama, K., Kopp, S., Chiba, P., and Ambudkar, S. V. (2007) Catalytic cycle of ATP hydrolysis by P-glycoprotein: evidence for formation of the E·S reaction intermediate with ATP-γ-S, a nonhydrolyzable analogue of ATP. *Biochemistry* **46,** 13787–13799
11. Vergani, P., Lockless, S. W., Nairn, A. C., and Gadsby, D. C. (2005) CFTR channel opening by ATP-driven tight dimerization of its nucleotide-binding domains. *Nature* **433,** 876–880
12. Sauna, Z. E., and Ambudkar, S. V. (2007) About a switch: how P-glycoprotein (ABCB1) harnesses the energy of ATP binding and hydrolysis to do mechanical work. *Mol. Cancer Ther.* **6,** 13–23
13. Verhalen, B., and Wilkens, S. (2011) P-glycoprotein retains drug-stimulated ATPase activity upon covalent linkage of the two nucleotide-binding domains at their C-terminal ends. *J. Biol. Chem.* **286,** 10476–10482
14. Verhalen, B., Ernst, S., Börsch, M., and Wilkens, S. (2012) Dynamic ligand-induced conformational rearrangements in P-glycoprotein as probed by fluorescence resonance energy transfer spectroscopy. *J. Biol. Chem.* **287,** 1112–1127
15. Moody, J. E., Millen, L., Binns, D., Hunt, J. F., and Thomas, P. J. (2002) Cooperative, ATP-dependent association of the nucleotide-binding cassettes during the catalytic cycle of ATP-binding cassette transporters. *J. Biol. Chem.* **277,** 21111–21114
16. Zoghbi, M. E., Fuson, K. L., Sutton, R. B., and Altenberg, G. A. (2012) Kinetics of the association/dissociation cycle of an ATP-binding cassette nucleotide-binding domain. *J. Biol. Chem.* **287,** 4157–4164
17. Chen, J., and Selvin, P. R. (1999) Thiol-reactive luminescent chelates of terbium and europium. *Bioconjug. Chem.* **10,** 311–315
18. Selvin, P. R. (2002) Principles and biophysical applications of lanthanide-based probes. *Annu. Rev. Biophys. Biomol. Struct.* **31,** 275–302
19. Bao, X., Lee, S. C., Reuss, L., and Altenberg, G. A. (2007) Change in permeant size selectivity by phosphorylation of connexin 43 gap-junctional hemichannels by PKC. *Proc. Natl. Acad. Sci. U.S.A.* **104,** 4919–4924
20. Leipe, D. D., Wolf, Y. I., Koonin, E. V., and Aravind, L. (2002) Classification and evolution of P-loop GTPases and related ATPases. *J. Mol. Biol.* **317,** 41–72
21. Sprang, S. R. (1997) G protein mechanisms: insights from structural analysis. *Annu. Rev. Biochem.* **66,** 639–678
22. Cha, A., Snyder, G. E., Selvin, P. R., and Bezanilla, F. (1999) Atomic scale movement of the voltage-sensing region in a potassium channel measured via spectroscopy. *Nature* **402,** 809–813
23. Knauf, P. A., and Pal, P. (2004) Use of luminescence resonance energy transfer to measure distances in the AE1 anion exchange protein dimer. *Blood Cells Mol. Dis.* **32,** 360–365
24. Posson, D. J., Ge, P., Miller, C., Bezanilla, F., and Selvin, P. R. (2005) Small vertical movement of a K^+ channel voltage sensor measured with luminescence energy transfer. *Nature* **436,** 848–851
25. Posson, D. J., and Selvin, P. R. (2008) Extent of voltage sensor movement during gating of shaker K^+ channels. *Neuron* **59,** 98–109
26. Rambhadran, A., Gonzalez, J., and Jayaraman, V. (2011) Conformational changes at the agonist-binding domain of the *N*-methyl-D-aspartic acid receptor. *J. Biol. Chem.* **286,** 16953–16957